AGU100 ADVANCING EARTH AND SPACE SCIENCE

JGR

Journal of Geophysical Research: Oceans

RESEARCH ARTICLE

10.1029/2018JC014487

Key Points:

- A new method to estimate return period extreme sea level values from satellite data is developed
- The outcomes from the application of the methodology to satellite altimetry data are validated using tide gauge records along the North American East Coast
- A climate variability analysis of extreme sea levels from monthly to decadal time scales is carried out

Correspondence to:
H. Lobeto,
lobetoh@unican.es

Citation:
Lobeto, H., Menendez, M., & Losada, I. J. (2018). Toward a methodology for estimating coastal extreme sea levels from satellite altimetry. *Journal of Geophysical Research: Oceans*, *123*, 8284–8298. https://doi.org/10.1029/2018JC014487

Received 24 AUG 2018
Accepted 23 OCT 2018
Accepted article online 1 NOV 2018
Published online 19 NOV 2018

Toward a Methodology for Estimating Coastal Extreme Sea Levels From Satellite Altimetry

H. Lobeto[1], M. Menendez[1], and I. J. Losada[1]

[1]Environmental Hydraulics Institute, Universidad de Cantabria, Santander, Spain

Abstract This work represents the first attempt to study the behavior of sea level extreme events nearshore using satellite altimetry data. A novel approach based on the application of a nonstationary extreme model to nontidal residual monthly maxima from remote data is presented. With the aim of countering the lack of accuracy, an extreme scale factor to correct satellite data is defined. The extreme scale factor depends on local morphology and its definition makes use of the information provided by 14 tide gauges along the North American East Coast. The methodology is validated using eight additional tide gauge records along the study region. Low differences on values associated to high return periods using satellite and tide gauge data input are found for all the validated locations. Besides, a regional study of the climate variability of extreme sea levels from satellite is also presented. The found climate patterns strongly agree with the historical climate variations from in situ data. Results show a great potential of this approach, especially at those locations where in situ information is not available.

Plain Language Summary Despite the great development of satellite altimetry during the last decade, satellite data have not been used to undertake an analysis of sea level extreme events nearshore yet. In this context, this work represents the first attempt to do that, presenting a methodology based on the use of satellite data to generate a coastal nontidal residual extreme sample and the application of a nonstationary statistical model to study its behavior. The methodology is applied along the North American East Coast, using 14 tide gauge records to compare the outcomes. Here we found differences in the extreme distribution obtained using remote and in situ data as input. Thus, with the aim of countering the lack of accuracy, an extreme scale factor to correct the extreme distribution from satellite data is defined. The application of the extreme scale factor at eight additional tide gauges allows to significantly reduce the error obtained using satellite data. Besides, an application of this methodology which consists in developing a climate study is also presented. The proposed methodology shows a great potential for its application with predictive purposes at those locations where there is not presence of tide gauges, which implies a huge impact for a wide range of applications.

1. Introduction

The rising population together with the change in natural defenses on coastal areas make them particularly vulnerable to the impact of extreme sea levels. In recent years there has been a growing interest on flooding and erosion impacts due to the effect of sea level rise and how it will enhance the occurrence of extreme sea levels (Wahl & Chambers, 2015). A correct characterization of the extreme sea level probability distribution is therefore essential for coastal protection.

Tide gauge (TG) stations have been considered as the main providers of information about sea level for more than a hundred years (e.g., San Francisco since 1854, Fort Denison since 1897). However, TGs have a series of limitations, such as (i) they only provide information restricted to mainland margins or ocean islands; (ii) their records are strongly conditioned by local morphology (e.g., estuaries and ports) and relative to the Earth crust, being affected by land movements (e.g., Peltier, 2001; Wöppelmann & Marcos, 2016); (iii) there is an irregular temporal and spatial coverage of the stations (most of them located in the northern hemisphere).

Despite all these issues, TG data provide valuable information and have been widely used to carry out studies about the influence of climate change effects on sea level. In this context, they have allowed to estimate not only global historical sea level rise trends (Jevrejeva et al., 2014), but also mean sea level local projections according to the scenarios raised by the Intergovernmental Panel on Climate Change (IPCC) (Kopp et al., 2014). Furthermore, although the influence of climate change on the frequency and

magnitude of storms is still a topic under debate, TG records have been used to clarify and deepen in this issue. The main conclusion derived from these studies was that the main influence factor is the global mean sea level rise (Menéndez & Woodworth, 2010; Tebaldi et al., 2012).

From 1992 onward, the development of satellite altimetry has given the possibility of carrying out new studies and improving our knowledge of the ocean. First, the open ocean, where this global source of information has been used as a trustful predictor of Mean Sea Level (MSL) (among other variables, e.g., significant wave height), allowing to estimate the historical sea level rise increasing trends (Church et al., 2013). Second, coastal regions, where the possibility of using this database for a period longer than 20 years offers the opportunity of complementing the information provided by TGs, especially at those coastline stretches where there are none (Vinogradov & Ponte, 2011).

In order to increase the accuracy of radar altimetry (especially in coastal areas), the Coastal Altimetry Community is focused on the improvement of the corrections applied to the radar pulse (Vignudelli et al., 2011). Despite there is still room for improvement, current corrections have already led to find a good agreement between in situ and remote data at the United Kingdom, giving optimistic prospects with regard to the use of remote data along the coast (Cipollini et al., 2017). Moreover, the Climate Change Initiative set up by the European Space Agency in 2010 (Quartly et al., 2017), which includes the definition of a consistent sea level data set through satellite altimetry measurements (among others Essential Climate Variables [ECV's]), has encouraged the improvement of altimetry corrections in order to maximize the accuracy of the database (Legeais et al., 2017).

Notwithstanding all these improvements, the information given by satellite altimeters has not been used yet to undertake an analysis of sea level extreme events on the coastal area. In this work we present a novel method to obtain the nontidal residual (NTR) extreme regime along the coast, based on the application of a nonstationary extreme model to monthly maxima from satellite measurements and taken into account the local morphology.

The paper is organized in six sections. Following the introduction, section 2 presents the data sources used in our analysis. Sections 3 and 4 are dealing with the methodology and its validation. The new methodology is applied along the North American East Coast to analyze extreme sea level variability and trends, a region characterized by a wide variety of extreme sea level conditions (i.e., Tropical and Extratropical cyclones). Finally, the most relevant conclusions are summarized.

2. Sea Level Data Sources

2.1. In Situ Observations

This work makes use of a set of 22 TG records along the North American East Coast (Figure 1) managed and distributed by the National Oceanic and Atmospheric Administration (NOAA). Information about both the observed sea level and predicted tide (based on a harmonic reconstruction) for each station is available at NOAA COOPS website (https://www.co-ops.nos.noaa.gov/products.html). The NTR component (NTR_{TG}) is obtained subtracting the predicted tide (NOAA harmonic analysis) from the observed water level. Consequently, the remaining NTR variable is mainly driven by meteorological and oceanographic processes and can be considered as a random variable of the climate system.

The criteria for the selection of the 14 TGs used to calibrate the method in the study region was based mainly on the existence of a quality control process, the temporal coverage (1993–2015, i.e., time span in which altimetry information is available), and the availability of continuous time series. Eight additional TGs are used to validate the method following similar criteria, although these stations show a higher number of gaps in their records.

2.2. Remote Observations

The operating principle of satellite altimetry consists in calculating the distance between the altimeter and a reference surface, recording the traveling time of the pulse from the antenna to the ocean and back again after being reflected. The magnitude and shape of the received waves give information about the reflecting surface, thereby allowing the recording, not only of sea level, but also of other variables such as significant wave height.

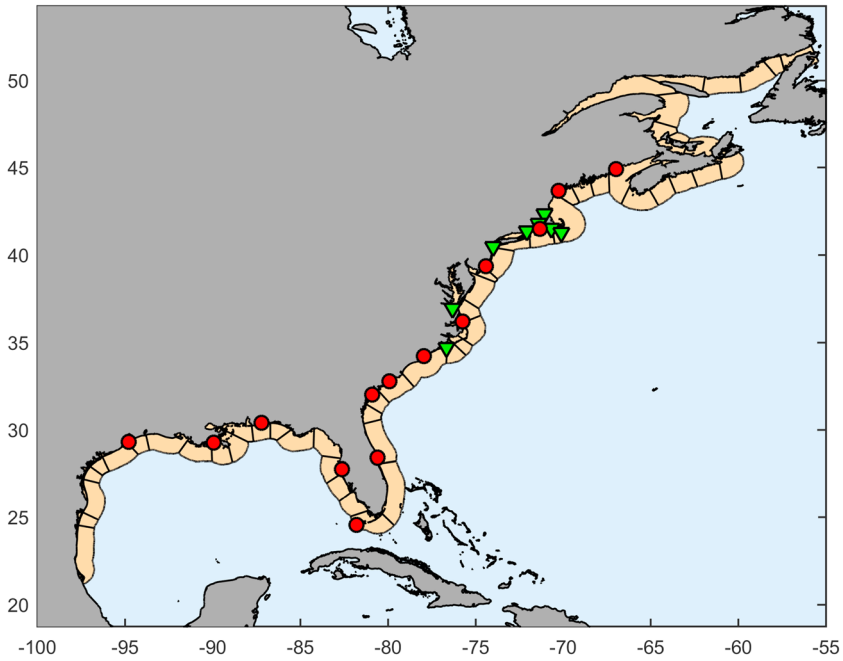

Figure 1. Tide gauge locations along the North American East Coast. Red dots show the stations considered to develop the methodology and green triangles those considered for validation. Orange zones represent the coastal areas defined to carry out a climate analysis using only satellite data.

The range recorded by the altimeter (R_{obs}) requires a series of corrections (Figure 2) which fall into two different groups. Range corrections consider the alteration of the radar speed and the actual scattering surface of the radar pulse. Geophysical corrections essentially consider different components of the sea level to identify the oceanic contribution to sea surface height (SSH) variations (Vignudelli et al., 2011). Range corrections include Dry Troposphere Refraction (*DTR*), the effect of dry gases on the radar pulse; Wet Troposphere Refraction (*WTR*), refraction due to the presence of water vapor in the troposphere; Ionosphere refraction (*IONO*), wave refraction in the ionosphere; Sea-State Bias correction (*SSB*), the bias of the range measurement due to the ocean wave troughs.

On the other hand, geophysical corrections include Dynamic Atmosphere Correction (*DAC*), the effect of pressure and wind; Tide Correction (*TIDES*), the tide component of sea level; and the Geoid Correction (*GEOID*), the difference between the reference surface and the geoid.

Thus, the corrected range (R_{corr}) can be obtained as

$$R_{corr} = R_{obs} + DTR + WTR + IONO + SSB \tag{1}$$

SSH referenced to the ellipsoid is related to the total height (*H*) of the altimeter through the following expression:

$$SSH = H - R_{corr} = H - (R_{obs} + DTR + WTR + IONO + SSB) \tag{2}$$

Moreover, *SSH* can be expressed as the sum of the geophysical corrections and the dynamic SSH (*DSSH*):

$$SSH = DSSH + GEOID + TIDES + DAC \tag{3}$$

$$DSSH = SSH - GEOID - TIDES - DAC \tag{4}$$

Note that it is possible to relate DSSH with all the corrections described as

$$DSSH = H - R_{obs} - DTR - WTR - IONO - SSB - GEOID - TIDES - DAC \tag{5}$$

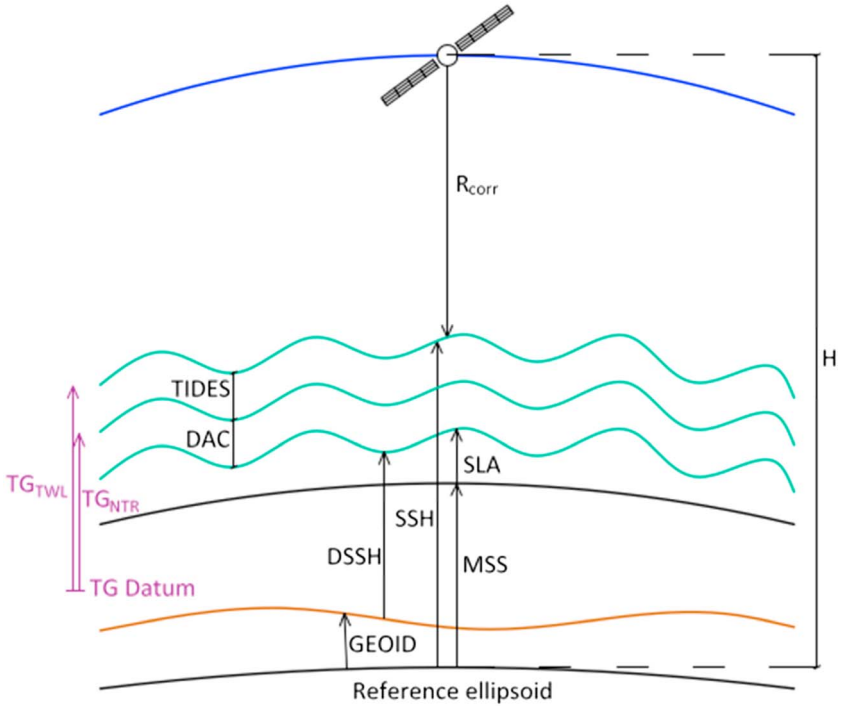

Figure 2. Corrections applied to the altimeter observations of SSH. TG record components are also included. TIDES = Tide Correction; DAC = Dynamic Atmosphere Correction; TG = Tide Gauge; NTR = Nontidal Residual; SSH = Sea Surface Height; DSSH = Dynamic SSH; SLA = Sea Level Anomaly; MSS = Mean Sea Surface; GEOID = Geoid Correction.

Finally, the reference level is changed by subtracting the mean sea surface (*MSS*). As a result, the variations of SSH due to oceanic processes (e.g., ocean currents) referenced to mean sea level are obtained, that is, the Sea Level Anomaly (*SLA*):

$$SLA = H - R_{obs} - DTR - WTR - IONO - SSB - TIDES - DAC - MSS. \quad (6)$$

For this work, satellite sea level information provided by the Copernicus Marine Environment Monitoring Service (CMEMS), in particular, the product *SEALEVEL_GLO_PHY_L3_REP_OBSERVATIONS_008_045*, which is available at the CMEMS webpage, is used. The selection of this data set is based on a preliminary analysis of several satellite products (CMEMS, RADS, and X-Track). CMEMS product is chosen due to the larger coastal sample values and higher correlations against in situ records. This product is processed by the DUACS multimission altimeter data processing system, integrating the along-track measurements of 14 satellite missions operating from 1992 to 2015. The result is an intercalibrated global data set of SLA. Further information about the processing system and the corrections applied for the generation of this product can be found in Pujol et al. (2016).

One of the main objectives of this work is to undertake a comparison between remote data and the NTR component obtained from in situ observations (NTR_{TG}). Thus, we applied a processing to the CMEMS SLA product in order to obtain an equivalent NTR database (NTR_{SAT}). Because CMEMS SLA data set includes the DAC, a reconstruction consisting in its readdition is required. To process the CMEMS database we used the DAC product originated from AVISO (Archiving, Validation and Interpretation of Satellite Oceanographic data) used to obtain the SLA data set. This is a global gridded product (0.25° × 0.25°) that provides 6-hourly information. The DAC is made of two constituents: low-frequency contribution for periods longer than 20 days, calculated through the use of the classical inverse barometer; and high-frequency contribution for periods shorter than 20 days, obtained as output of the MOG2D model (Carrère & Lyard, 2003). Finally, an along-track NTR_{SAT} data set is obtained as the sum of DAC and SLA.

$$NTR_{SAT} = SLA + DAC \quad (7)$$

3. Methodology

Here a novel method to process the NTR_{SAT} database and study the behavior of sea level extreme events along the coast is developed. The first step consists of selecting the data sample, which serve as input to undertake the subsequent extreme analysis. In order to estimate return sea levels (e.g., extreme value associated to 20-year return period) from a random and nonstationary NTR variable, a time-dependent statistical extreme model is applied. An *extreme scale factor* (ESF) to correct the return sea level estimates from satellite data is defined. The ESF is based on comparisons between satellite and in situ observations and takes into account different geographical and morphological characteristics. Finally, the proposed approach is validated by a comparison of the estimated return levels from satellite against TG records.

3.1. The Coastal Extreme Sample

As mentioned in section 2.2, the built along track NTR_{SAT} database is heterogeneous in space and time. A method to select the data sample input for the following analysis is therefore required. Two different selecting methods are proposed. In order to carry out a comparison with in situ observations, a data sample associated with a specific TG is selected first. A second selection process is needed in order to apply the approach for a specific coastal area.

For a particular TG, the selection of a related NTR_{SAT} data set is based on the existing correlation between both data sources in the vicinity of the station. With the aim of making both data sets directly comparable, the first step consists of building pairs using each NTR_{SAT} measurement and the closest in time NTR_{TG} value.

The surrounding area of a TG is delimited by a 7.5° radius circle whose center is the position of the station. This area is gridded with a 0.25° × 0.25° mesh so that the correlation value in each grid-point is calculated as the correlation coefficient between all the remote-in situ pairs in a 0.25° radius circle. Figure 3 shows two maps with the correlation values obtained after applying this method to Atlantic City and Galveston Pier stations. It can be observed that higher distance to the TG results in lower correlation values, as well as different correlation patterns depending on the geographic location.

After the analysis of the correlation maps for the 14 TG sites used, we set a correlation threshold of 0.50, so that the selected remote measurements associated to a TG are those whose grid-points have higher correlation coefficients (i.e., coastal marine areas within thick black line of Figure 3). The coastal satellite data selected within the 0.5 correlation contour have a mean time resolution close to hourly. Once the selection area for each TG is defined, we select the in situ and remote data sets used to feed the statistical extreme model. Monthly maxima from TG recorded values for the period 1993–2015 are selected. Besides, in order to avoid spurious maxima values, only those months including samples over 60% of the recorded hourly values are taken into account (Menéndez & Woodworth, 2010).

A similar method is applied to NTR_{SAT} data. First, the monthly average number of remote measurements available during the period 1993–2015 for the 14 TG surrounding areas is estimated (N_{SA}). After that, monthly maxima for each station are selected, considering only those months with a number of samples higher than $0.6{\cdot}N_{SA}$. As can be appreciated in Figure 4, some maxima storm surge events recorded by the TG could be missed, while other extreme events can have associated a higher satellite value.

To develop a climate analysis 500-km long coastal stretches are defined along the region. The analysis of each stretch is developed using all the remote measurements in its adjacent coastal zone (orange zones at Figure 1). The width of these adjacent areas is set 50 km in the offshore direction considering an average distance between the coast and the 0.50 correlation contour obtained from the correlation maps. Finally, monthly maxima in each coastal area are selected. To do that, we first obtain the monthly average number of measurements at each area (N_1, N_2…N_M, where M is the number of coastal areas). Then, we calculate the average number between all the areas (N_T). Finally, only those months with a number of data higher than the 60% of N_T are selected.

3.2. Statistical Model

3.2.1. Time-Dependent GEV Model

According to Fisher-Tippet theorem (Galambos, 1987), the maxima sample of Independent and Identically Distributed random variables appropriately normalized converge to a Generalized Extreme Value distribution

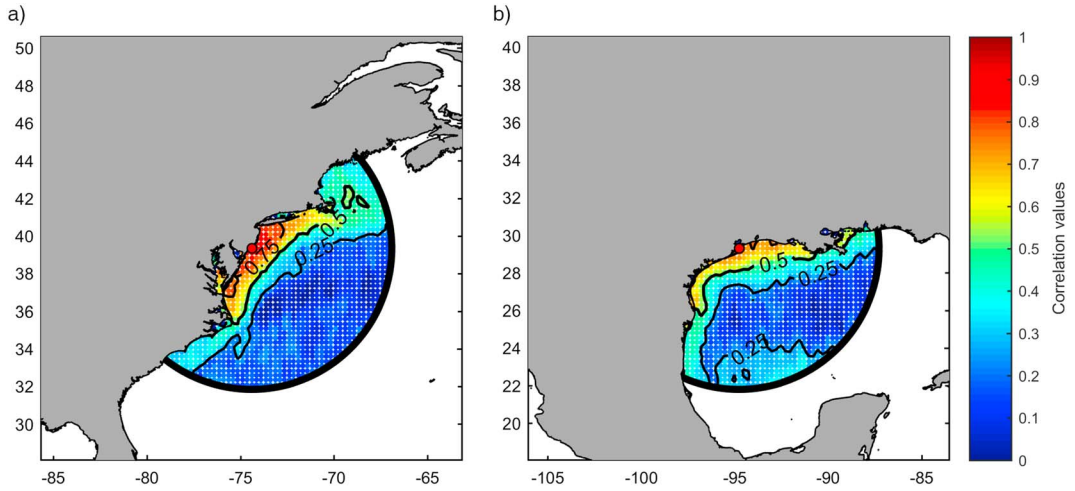

Figure 3. Correlation value at each mesh node for (a) Atlantic City tide gauge (New Jersey) and (b) Galveston Pier tide gauge (Texas). The 0.25, 0.50, and 0.75 correlation contours are also represented. The location of the station is marked with a red circle.

(GEVD). Depending on the shape of the distribution tail, it can belong to three different families: Weibull, Gumbel, and Fréchet. A nonstationary GEV distribution function (F_t) can be expressed as

$$F_t(z) = \begin{cases} \exp\left\{-\left[1+\xi\left(\frac{z-\mu(t)}{\psi}\right)\right]^{-\frac{1}{\xi}}\right\} & \xi \neq 0 \\ \exp\left\{-\exp\left[-\left(\frac{z-\mu(t)}{\psi}\right)\right]\right\} & \xi = 0 \end{cases}, \tag{8}$$

where $\mu(t)$ is the time-dependent location parameter, ψ is the scale parameter, and ξ is the shape parameter, whose sign informs about the tail of the distribution ($\xi < 0$, $\xi = 0$, $\xi > 0$, for the Weibull, Gumbel, and Fréchet family, respectively).

With the aim of introducing the nonstationary behavior of the NTR climate variable and providing the model with a large maxima sample, monthly maxima are used as block maxima sample and parametric time-

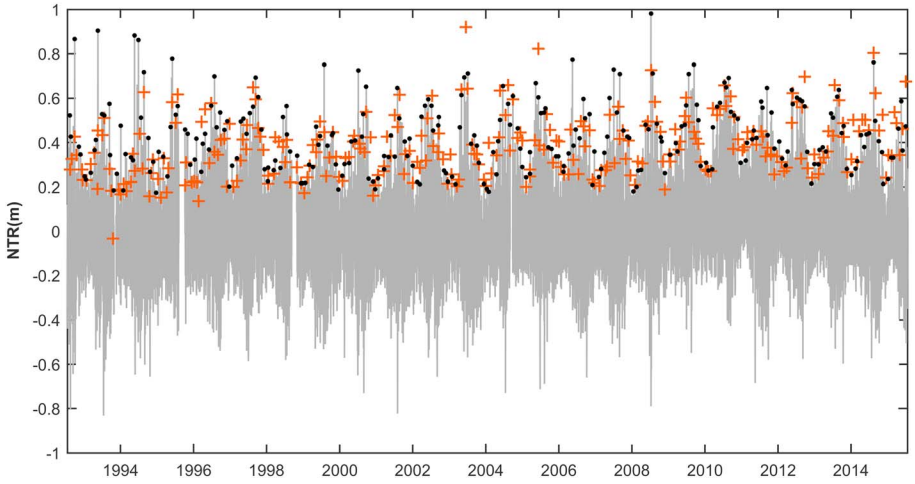

Figure 4. NTR record from Eastport tide gauge. Black dots represent monthly maxima from tide gauge data and orange crosses represent monthly maxima from satellite data. NTR = Nontidal Residual.

dependent terms are included to consider underlying climate variations into the extreme model. Climate variations are considered in the location parameter $\mu(t)$, which implies that the statistics from the distribution change over time. The calculation of NTR values associated to a R-year return period for a certain time (e.g., 2018 t_i year) in a nonstationary GEVD ($\overline{z}_R$) can be undertaken using the expression shown in equation (9).

$$1-{}^{1}\Big/_{R}=\begin{cases}\exp\left\{-\int_{t_i}^{t_i+T}\left[1+\xi\left(\dfrac{\overline{z}_R-\mu(t)}{\psi}\right)\right]^{-\frac{1}{\xi}}dt\right\} & \xi\neq 0\\ \exp\left\{-\int_{t_i}^{t_i+T}\exp\left[\dfrac{\mu(t)-\overline{z}_R}{\psi}\right]dt\right\} & \xi=0\end{cases}, \tag{9}$$

where T is the time variable with a year unit scale.

3.2.2. Model Selection

As it was briefly mentioned in the previous section, the statistical extreme model takes into account climate variations through the location parameter as a parametric model. Three climate scale variations are included: a sum of sine functions representing seasonal effects, an exponential term representing long-term trends, and a covariate representing interannual variations due to regional climate circulation patterns (e.g., Arctic Oscillation, AO).

3.2.2.1. Seasonal Variations

The study of seasonal variations in extreme statistical analysis of climate parameters has been already faced in previous works. Menéndez and Woodworth (2010) applied a statistical extreme model (GEVD) to sea level extreme events from TGs considering seasonal variations, obtaining a clear agreement with monthly maxima and illustrating how these events can vary throughout the year.

In this work seasonal variability is modeled introducing an annual cycle and the possibility (as long as the mathematical significance demands it) of the two consecutive subharmonics as sinusoidal functions. Therefore, different combinations of these three cycles (2^3 combinations) allow representing the specific seasonality locally:

$$\mu_s(t)=\sum_{i=1}^{3}\left[\beta_{2i-1}\cdot\cos\left(2^i\pi t\right)+\beta_{2i}\cdot\sin\left(2^i\pi t\right)\right], \tag{10}$$

where β_i is the amplitude of the harmonics and t is given in years.

3.2.2.2. Long-Term Trend

To consider long-term variability, a trend is included in the model. The trend is computed using an exponential time dependence to include a possible acceleration of the long-term trend. Thus, the model is able to simulate the increase or decrease in the magnitude of NTR extreme events.

$$\mu_{trend}=\beta_0\cdot\exp(\beta_{LT}\cdot t). \tag{11}$$

Note that if β_{LT} is very low, the growth tends to be linear, allowing to estimate the trend as $\beta_0\cdot\beta_{LT}$ (slope of the line).

3.2.2.3. Interannual Oscillations

Interannual climate patterns, often represented by teleconnection indices, are also present in sea level extreme events. Three relevant climate indices (CIs) have been selected to investigate the influence of coupled ocean-atmosphere modes in extreme water level changes: Niño 3–4 as a descriptor of El Niño–Southern Oscillation mean conditions; the AO as a reliable descriptor of the winter climate in the northern hemisphere and highly correlated with the North Atlantic Oscillation and the Tropical North Atlantic (TNA) which describes the climate in the tropical zone of the Atlantic Ocean (Enfield et al., 1999). Niño 3–4 and AO are selected from the NOAA-National Weather Service (data available at http://www.cpc.ncep.noaa.gov). TNA is selected from the Ocean Observations Panel for Climate (data available at https://stateoftheocean.osmc.noaa.gov). Thus, these patterns are introduced in the extreme model through their monthly indices as a covariate ($cvte(t)$).

$$\mu_{cvte} = \beta_{CVTE} \cdot cvte(t), \tag{12}$$

where β_{CVTE} is the estimated covariate coefficient in centimeter per CI unit.

Considering all the climate variations, the location parameter can be expressed as follows:

$$\mu(t) = \beta_0 \cdot \exp(\beta_{LT} \cdot t) + \beta_1 \cdot \cos(2\pi t) + \beta_2 \cdot \sin(2\pi t) + \beta_3 \cdot \cos(4\pi t) + \beta_4 \cdot \sin(4\pi t) + \beta_5 \cdot \cos(8\pi t) + \beta_6 \cdot \sin(8\pi t) + \beta_{cvte} \cdot cvte(t). \tag{13}$$

The selection of the optimal extreme model follows an orderly and efficient flow. It consists of the introduction one by one of the different temporary variations described previously with the main goal of obtaining the combination that fits better to the NTR monthly maxima. The comparison between models is based on the maximum likelihood ratio test and the principle of parsimony, that is, minimizing the number of degrees of freedom to avoid an overparameterization of the model (Coles, 2001).

At a first stage, the location parameter just considers the seasonal variability. In order to find the simplest model, a forward algorithm starting from a stationary model is used (model m_0), testing different combinations of sine functions until the optimal is reached (model m_1).

Next step consists of introducing the trend term in the location parameter. If it is significant (within the 95% confidence interval), it will be included in model m_2. Otherwise m_2 will be equal to m_1. Finally, based on m_2, the same process is made to define model m_3. In this case, introducing a CI as a covariate in $\mu(t)$. Each of the three mentioned CIs were analyzed independently. Thus, m_3 is the optimal model which integrates all the climate variations and represents better the climate variability in the coastal area.

3.3. Inference for Return Level

Following the application of the statistical model to all the stations, we compare the extreme distribution obtained using TGs and altimetry data. Thus, $\varnothing_{Ri}$ is defined as the ratio between in situ $\left(z_{Ri}^{TG}\right)$ and remote $\left(z_{Ri}^{SAT}\right)$ NTR values associated to a return period R_i (in years) at a certain station (equation (14)). Note that there are not significant changes in $\varnothing$ for different R_i and for the 14 stations analyzed (Figure 5).

$$\varnothing_{Ri} = \frac{z_{Ri}^{TG}}{z_{Ri}^{SAT}}. \tag{14}$$

Given those small changes, $\overline{\varnothing_j}$ is defined as the mean ratio for a station j:

$$\overline{\varnothing_j} = \frac{1}{N} \sum_{Ri=10}^{Ri=50} \frac{z_{Ri}^{TG}}{z_{Ri}^{SAT}}. \tag{15}$$

Thus, $\overline{\varnothing_j}$ ranges from 0.50 to 2.75, being in most cases higher than the unit ($z_{Ri}^{TG} > z_{Ri}^{SAT}$) for the study area. The differences between $\left(z_{Ri}^{TG}\right)$ and $\left(z_{Ri}^{SAT}\right)$ can be related to morphological and geographical characteristics at the location of study. NTR sea level signal over coastal areas against open ocean areas can indeed be sensitive to amplifications/decreases due to depth-limitations and nonlinear interactions between individual sea level components. Consequently, in order to account for these differences and to correct the NTR extreme distribution from satellite data, an ESF is defined in this work. After checking a number of possible factors to define the ESF, two different constituents are found to be significant:

1. **Coastal exposure constituent (K_{EP})**: This constituent takes into consideration the exposure of a specific location to the open ocean (C_{EP}). It seeks to reflect, first, the fact that closer to the coast a lower number of altimeter measurements are available, especially in rugged coastlines and sheltered estuaries. Second, the amplification experienced by storm surge as it approaches the coast, in particular at those locations where the pathway from the open ocean to the coast is shallow, narrow, and winding due to local morphology (e.g., presence of islands) or human intervention (e.g., port infrastructures).

   C_{EP} is calculated as the average ray length between the location of study and the first obstacle encountered considering more than 1,000 rays (Figure 6a). Because small obstacles (e.g., islands) have no

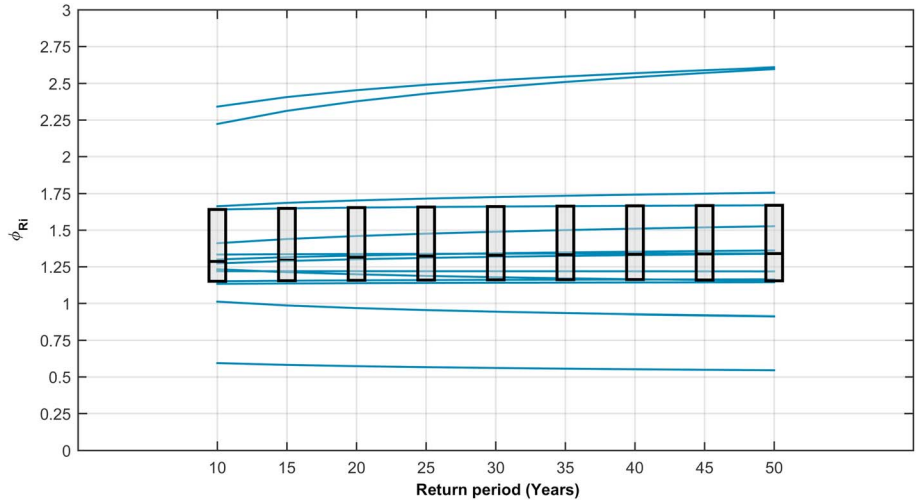

Figure 5. Lines represent $\varnothing_{Ri}$ for the 14 stations of study from 10- to 50-years return period. Boxes represent 0.25, 0.50, and 0.75 quantile for each return period considered.

significant effect in the propagation of a long wave, those with an area smaller than 1 km^2 are not considered in the calculation algorithm. C_{EP} is exponentially related with $\overline{\varnothing j}$ though the expression shown in equation (16) and represented in Figure 6c:

$$K_{EP} = 2.046 \cdot \exp(-C_{EP} \cdot 1.876). \quad (16)$$

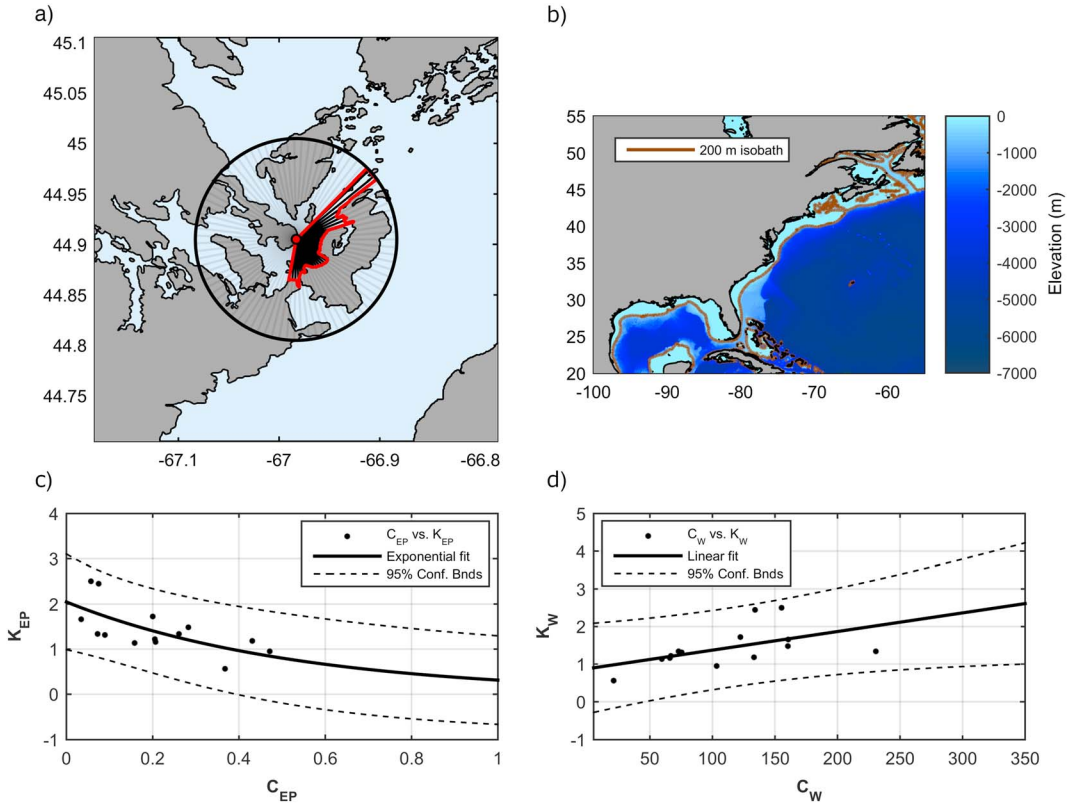

Figure 6. a) Coastal exposure constituent scheme, (b) bathymetry and 200 m isobaths in the area of study, (c) exponential relationship between C_{EP} and K_{EP}, (d) linear relationship between C_W and K_W.

It can be concluded that TGs with less exposure to the open ocean require a higher coastal exposure constituent values.

2. **Continental shelf width constituent (K_W):** This constituent relates to the width of the continental shelf at the location of study (C_W) and $\overline{\varnothing j}$. It represents the loss of precision of radar altimetry in the shelf. C_W is obtained as the minimum width of the shelf at the location of study (Figure 6b).

   In this case, there is a linear relationship between both variables (equation (17)).

$$K_W = C_W \cdot 0.004954 + 0.8776. \tag{17}$$

   This relationship implies that the higher the width of the continental shelf, the higher the shelf constituent, that is, a wider shelf implies higher differences between z_{Ri}^{TG} and z_{Ri}^{SAT}.

Thus, ESF can be obtained as a weighted combination of both constituents:

$$ESF = w_{EP} \cdot K_{EP} + w_W \cdot K_W, \tag{18}$$

where w_{EP} and w_W are the weights associated to K_{EP} and K_W.

The application of the ESF to z_{Ri}^{SAT} results in a corrected satellite NTR value associated to a return period R_i (in years) $z_{Ri}^{SAT'}$ (equation (19)). Therefore, a corrected ratio $\varnothing'_{Ri}$ is obtained (equation (20)).

$$z_{Ri}^{SAT'} = ESF \cdot z_{Ri}^{SAT}, \tag{19}$$

$$\varnothing'_{Ri} = \frac{z_{Ri}^{TG}}{z_{Ri}^{SAT'}}. \tag{20}$$

In order to define the optimal weight distribution, the combination that minimized the Mean Square Error between $\varnothing'_{Ri}$ and the unit is to be found. Finally, we obtained a higher contribution of the coastal exposure constituent (65%) with respect to the shelf width.

$$ESF = 0.65 \cdot K_{EP} + 0.35 \cdot K_W. \tag{21}$$

4. Validation of the Methodology

The validation of the methodology is carried out with the information provided by eight TG records not used previously in the regression model of the ESF and placed as well along the North American East Coast (Figure 1). After the quality control and following each stage described in *Section* 3, the methodology is applied to NTR_{SAT} and NTR_{TG} data sets at these locations.

Making use of the relationship described in equation (21), ESF is calculated for all the validation sites. Its application to z_{Ri}^{SAT} allows to significantly reduce the differences with those obtained using in situ observations ($z_{Ri}^{TG} \cong z_{Ri}^{SAT'}$), which implies that $\varnothing'_{Ri}$ approaches to unit in all stations analyzed (Figure 7c). Before applying the correction based on ESF, $\overline{\varnothing}$ was always above unit, with values ranging between 1.5 and 2.5. After applying ESF, however, $\overline{\varnothing}'$ ranges between 0.8 and 1.25 (i.e., relative error lower than 25%), with a mean relative error of about 10%.

As an example, Figures 7a and 7b show the return level plots at two validation locations, Beaufort (NC) and Providence (RI). Note that in both cases the corrected return level plot from altimetry almost matches the return level plot from in situ measurements not only in magnitude, but also in shape. Besides, 95% confidence bounds of the return values from the TG record are also shown in Figures 7a and 7b.

5. Climate Variations

In this section the proposed methodology is applied along the North American East Coast. A climate analysis at different time scales is carried out, providing (i) information of climate variability patterns for the coastal

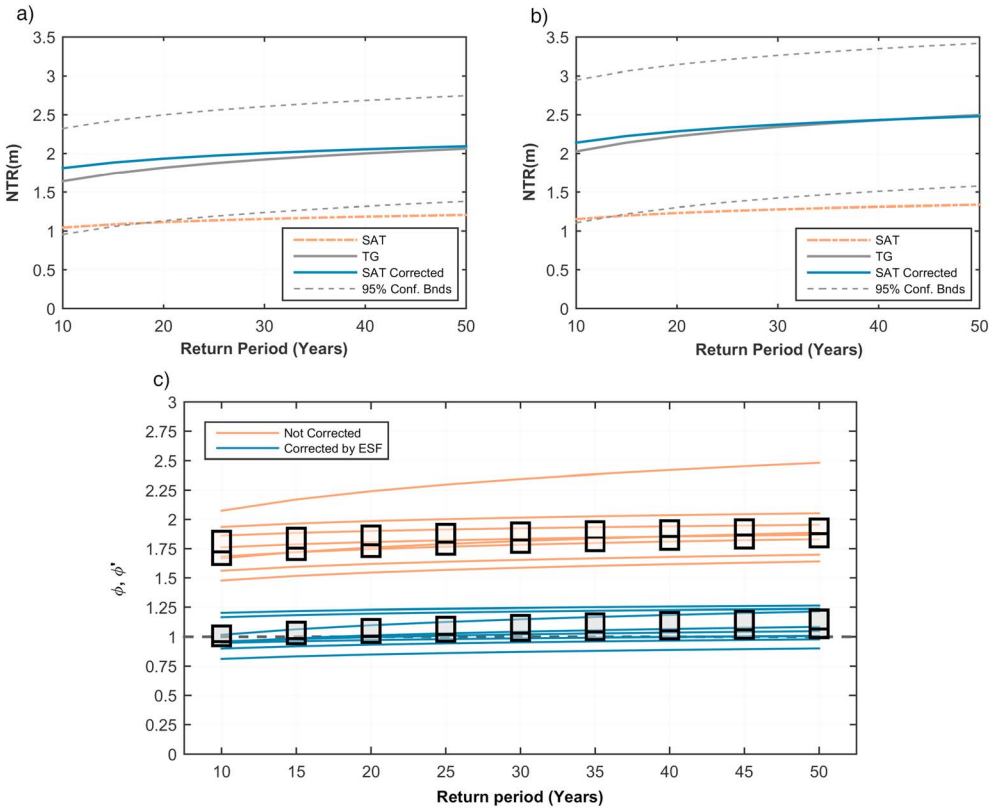

Figure 7. Return level plots obtained from satellite data, TG data and satellite data corrected by ESF for (a) Beaufort tide gauge and (b) Providence tide gauge; both figures include 95% confidence bounds from TG data; (c) $\varnothing$ (orange lines) and $\varnothing'$ (blue lines) values for 10- to 50-years return levels in eight stations. Boxes represent 0.25, 0.50, and 0.75 quantiles for each return period considered. NTR = Nontidal Residual; TG = Tide Gauge; ESF = Extreme Scale Factor.

area, and (ii) another way to validate that climate extremes estimated under this method provide similar climate information than TG extreme analysis.

5.1. Seasonal Dependence

The introduction of seasonality in the extreme model allows to reproduce the behavior of NTR extreme values within the year. The evidence of the nonstationarity in sea level extreme events have been proved in previous studies at global (Menéndez & Woodworth, 2010), regional (Marcos & Woodworth, 2017), and local scales (Méndez et al., 2007; Menendez et al., 2009).

In this context, Figure 8 shows for each coastal zone which is the month with higher probability of presenting higher NTR extreme events. This assessment was made by estimating the timing of the largest 50-year return values. Two clear areas can be distinguished. The northern coast, which climate is mainly controlled by the occurrence of extratropical cyclones, shows a clear winter pattern with higher probability of sea level extreme events from November to February. The southern coast is affected by the impact of tropical cyclones (TC's), provoking that the months with the greatest probability of presenting extreme events are those which belong to the TC season (i.e., from June to October). The storminess pattern found agrees with previous works based on TG data sets, pointing out the existence of a storm activity uniformity along the North American East Coast. While stations located northernmost are highly affected by extratropical cyclones activity, the influence of TCs becomes more significant at those located southernmost (Wahl & Chambers, 2015; Zhang et al., 2000).

5.2. Interannual Variability

Interannual and decadal variations are present in extreme surge events. The consideration of climate oscillations in the statistical model allows us to analyze the influence of each teleconnection pattern in the persistence of NTR extreme events along the coast of study.

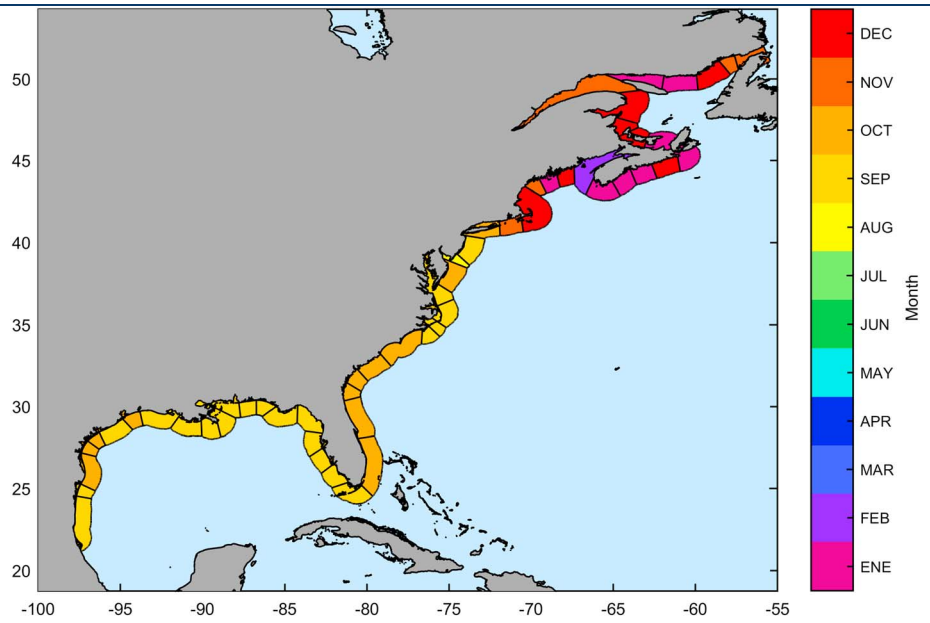

Figure 8. Month with higher probability of presenting higher nontidal residual extreme events.

Results show a strong correlation between the negative phase of AO and NTR extreme events along the northern part of the coast of study (Figure 9a), meaning that there is a higher probability of NTR extreme events during this phase. Moreover, results obtained after applying the statistical extreme model to the information provided by TGs agree with those obtained using remote information. Thus, Figure 9b shows a strong correlation with AO negative phase (significance level higher than 95%) in all the stations analyzed along the coastal stretch from Atlantic City TG to Eastport TG.

In fact, previous studies based on TG records using the skew surge parameter (Marcos & Woodworth, 2017) or composite sea level (Wahl & Chambers, 2015) have already demonstrated that extreme sea levels in this part of the world are dominated by North Atlantic Oscillation and AO climate patterns, showing a strong correlation with their negative phase.

Two different areas show an important correlation with TNA but with opposite sign (Figure 10a). A positive correlation is found with this teleconnection index from 35 to 45°N, reaching values of 5 cm per CI unit in the covariate coefficient. The Atlantic coast located from 25 to 35°N, however, has a negative correlation with TNA, presenting also lower absolute values. Finally, along Mexican Gulf coastline it is observed a positive

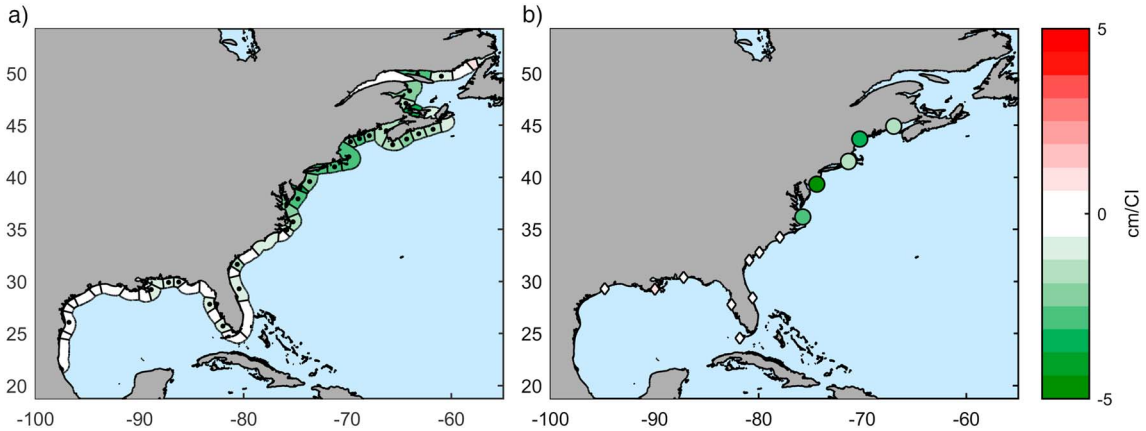

Figure 9. (a) Arctic Oscillation index covariate coefficient values in centimeter per CI units for each coastal zone analyzed, a black dot implies significance >75%. (b) Arctic Oscillation index covariate coefficient values in centimeter per CI units for each tide gauge considered in the definition of the methodology. Big circles markers imply a significance >95%, small circle markers imply a significance >75%, and small diamond markers indicate a significance <75%. CI = Climate Index.

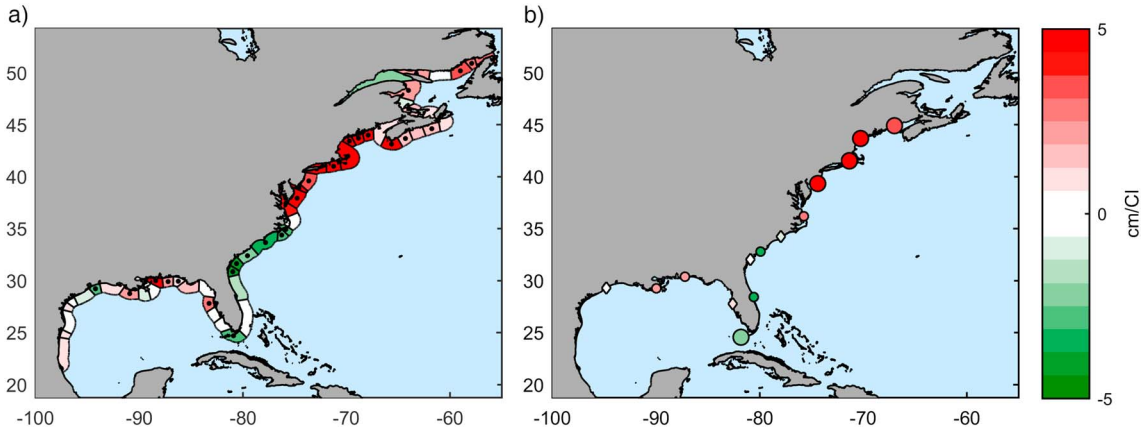

Figure 10. (a) Tropical North Atlantic index covariate coefficient values in centimeter per CI units for each coastal zone analyzed, a black dot implies significance >75%. (b) Tropical North Atlantic index covariate coefficient values in centimeter per CI units for each tide gauge considered in the definition of the methodology. Big circles markers imply a significance >95%, small circle markers imply a significance >75%, and small diamond markers indicate a significance <75%. CI = Climate Index.

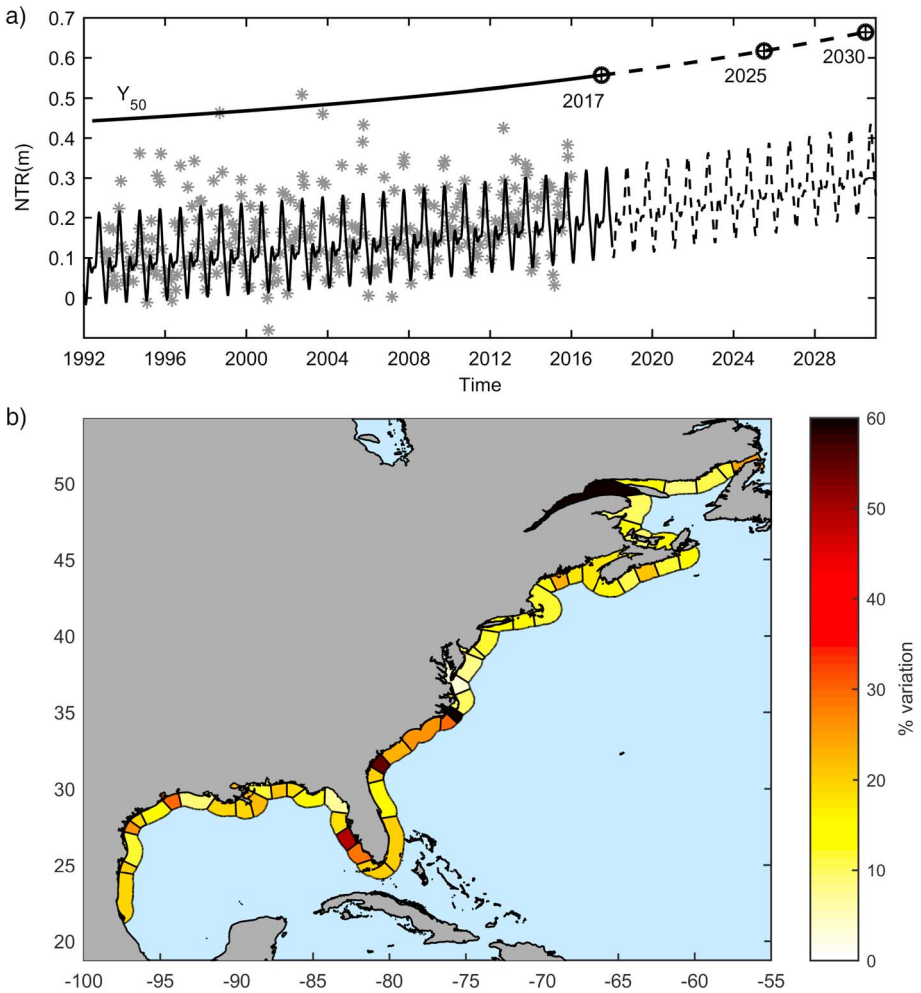

Figure 11. (a) NTR monthly maxima from satellite (dots), time-dependent Generalized Extreme Value distribution location parameter, and estimated rise of the 50-year return level for a coastal area. (b) Estimated variation (%) of the 50-year return period NTR between 2017 and 2030. NTR = Nontidal Residual.

correlation with TNA but less intense in comparison with the other two zones already described. Consistently with previous climate patterns, there is a high agreement between the results obtained from in situ and remote information.

Despite there is not a continuous and strong correlation between El Niño–Southern Oscillation and the NTR_{SAT} monthly maxima (Figure not shown), there are several coastal areas with a significant positive correlation (i.e., La Niña phase). Covariate values on these area range between 0.5 and 2 cm per CI unit. The results obtained along the coast using in situ measurements (Wahl & Chambers, 2015) agree with the previous ones, showing mainly a positive correlation along South and North Carolina coastline and the Gulf of Mexico. Several studies (Marcos & Woodworth, 2017; Menéndez & Woodworth, 2010) have already shown a correlation between La Niña phase and the occurrence of extreme events in the southern East Coast, mainly hit by the impact of TC's (see section 5.1).

5.3. Long-Term Trends

The long-term trends of NTR monthly maxima are introduced in the model as an exponential function (Figure 11b). Figure 11a shows the variation of the 50-year return period NTR between 2017 and 2030 (a 14-year period) considering the recent historical rise. Note that the coastline stretch from North Carolina to Florida is the one with a higher expected rise in NTR monthly maxima, reaching values close to 60% variation. These results are consistent with those presented by Menéndez and Woodworth (2010), where the highest trends along the U.S. East Coast were found at TGs located in this region.

6. Concluding Remarks

In this work an approach to address the assessment of NTR extreme events through the use of satellite altimetry data is described.

Despite the fast development of satellite altimetry during the last decade, nowadays it is still not possible to get access to a NTR database nearshore. A method to generate a satellite NTR data set (NTR_{SAT}) based on the use of along track satellite data is proposed. Despite radar measurements lose accuracy nearshore, correlation values higher than 0.75 between NTR_{SAT} and NTR from TG data (NTR_{TG}) are obtained around the station in most of the cases analyzed (Figure 3). High correlation values show a good agreement between the behaviors of both data sets in the vicinity of the coast.

A novel methodology to process satellite altimetry data in the coastal zone is presented. It is based on the application of a nonstationary statistical extreme model (GEVD) to NTR_{SAT} data set. With the aim of countering the lack of accuracy and the reduced number of satellite data, monthly maxima are used as statistical model input (Figure 4). It is necessary, however, to correct the satellite data so that an *ESF* is defined. ESF depends on local morphology considering the coastal exposure and the continental shelf width (Figure 6) and its definition makes use of the information provided by 14 TGs along the North American East Coast. ESF correction consists in its application to modify the NTR_{SAT} extreme distribution.

The validation of the methodology is carried out through a comparison with data provided by eight additional TGs along the coast of study. The correction with ESF at these locations allows to significantly reduce the differences between return level plots obtained using remote and in situ information from a mean relative error of around 86% to around 10% (Figure 7c).

The application of a nonstationary statistical extreme model to NTR monthly maxima from satellite altimetry allows to successfully carry out a climate study along the coastal region, taking into consideration variations at different time scales (seasonal, interannual, and long-term trends). In fact, results show a clear agreement between climate patterns obtained using in situ and remote data.

The main outcomes from this work are first, a methodology to provide information on sea level extremes in coastal areas where in situ measurements are not available by using satellite data corrected with a local ESF, dependent on coastal morphology. Second, the application of a nonstationary statistical model (GEVD) to satellite NTR monthly maxima, allowing to develop applications such as carrying out a coastal climate study of extreme sea levels.

The proposed methodology shows a great potential for its application with predictive purposes at those locations where there are not any provider of in situ observations such as TGs, which implies a huge impact for a

wide range of coastal applications. We must state that the present work represents only the first step in the development of a methodology to study sea level extremes using information provided by satellite altimetry. Moreover, promising results obtained during this work make us looking forward to extend this methodology at global scale, considering not only NTR component, but also total the water level, and extending the relationships to define ESF to a wider range of coastal areas (e.g., Tropical and Extratropical regions, mainland and open ocean islands).

Acknowledgments
M. Menendez and H. Lobeto acknowledge the financial support from the Ramon y Cajal Program (RYC-2014-6469). The work reported here was partially supported by the Spanish Government through the grant PORTIO (BIA2015-70644-R); project ECLISEA, part of ERA4CS, an ERA-NET initiated by JPI Climate, and funded by UC-IHC, HZG, BRGM, NCSRD, and CNRS and co-funding by the European Union (Grant 690462), and the US DOD Strategic Environmental Research and Development Program (SERDP Project RC-2644). The access to CMEMS and NOAA data enabled the development and validation of the method. Supporting data are included as an XLSX file named supData-lobetoetal.

References

Carrère, L., & Lyard, F. (2003). Modeling the barotropic response of the global ocean to atmospheric wind and pressure forcing - comparisons with observations. *Geophysical Research Letters*, *30*(6), 1275. https://doi.org/10.1029/2002GL016473

Church, J. A., Clark, P. U., Cazenave, A., Gregory, J. M., Jevrejeva, S., Levermann, A., et al. (2013). IPCC WG1AR5 Chapter 13 Sea level change. Climate Change 2013: The physical science basis. Contribution of Working Group I to the Fifth Assessment Report of the Intergovernmental Panel on Climate Change. https://doi.org/10.1017/CB09781107415315.026

Cipollini, P., Calafat, F. M., Jevrejeva, S., Melet, A., & Prandi, P. (2017). Monitoring sea level in the coastal zone with satellite altimetry and tide gauges. *Surveys in Geophysics*, *38*(1), 33–57. https://doi.org/10.1007/s10712-016-9392-0

Coles, S. G. (2001). An introduction to statistical modeling of extreme values. *Springer Series in Statistics*. https://doi.org/10.1007/978-1-4471-3675-0

Enfield, D. B., Mestas-Nuñez, A. M., Mayer, D. A., & Cid-Serrano, L. (1999). How ubiquitous is the dipole relationship in tropical Atlantic sea surface temperatures? *Journal of Geophysical Research*, *104*, 7841–7848. https://doi.org/10.1029/1998JC900109

Galambos, J. (1987). The asymptotic theory of extreme order statisticsMalabar, Fla.: R.E. Krieger Pub. Co. Retrieved from file://catalog.hathitrust.org/Record/001301803

Jevrejeva, S., Moore, J. C., Grinsted, A., Matthews, A. P., & Spada, G. (2014). Trends and acceleration in global and regional sea levels since 1807. *Global and Planetary Change*, *113*, 11–22. https://doi.org/10.1016/J.GLOPLACHA.2013.12.004

Kopp, R. E., Horton, R. M., Little, C. M., Mitrovica, J. X., Oppenheimer, M., Rasmussen, D. J., et al. (2014). Probabilistic 21st and 22nd century sea-level projections at a global network of tide-gauge sites. *Earth's Future*, *2*(8), 383–406. https://doi.org/10.1002/2014EF000239

Legeais, J.-F., Ablain, M., Zawadzki, L., Zuo, H., Johannessen, J. A., Scharffenberg, M. G., et al. (2017). An improved and homogeneous Altimeter Sea level record from the ESA Climate Change Initiative. *Earth System Science Data Discussions*, 1–35. https://doi.org/10.5194/essd-2017-116

Marcos, M., & Woodworth, P. L. (2017). Spatiotemporal changes in extreme sea levels along the coasts of the North Atlantic and the Gulf of Mexico. *Journal of Geophysical Research: Oceans*, *122*, 7031–7048. https://doi.org/10.1002/2017JC013065

Méndez, F. J., Menéndez, M., Luceño, A., & Losada, I. J. (2007). Analyzing monthly extreme sea levels with a time-dependent GEV model. *Journal of Atmospheric and Oceanic Technology*, *24*, 894–911. https://doi.org/10.1175/JTECH2009.1

Menendez, M., Mendez, F. J., & Losada, I. J. (2009). Forecasting seasonal to interannual variability in extreme sea levels. *ICES Journal of Marine Science*, *66*(7), 1490–1496. https://doi.org/10.1093/icesjms/fsp095

Menéndez, M., & Woodworth, P. L. (2010). Changes in extreme high water levels based on a quasi-global tide-gauge data set. *Journal of Geophysical Research*, *115*, C10011. https://doi.org/10.1029/2009JC005997

Peltier, W. R. (2001). Global glacial isostatic adjustment and modern instrumental records of relative sea level history. In B. C. Douglas, M. S. Kearney, & S. P. Leatherman (Eds.), *Sea level rise* (Vol. 75, pp. 65–95). San Diego, CA: Academic Press. https://doi.org/10.1016/S0074-6142(01)80007-3

Pujol, M. I., Faugère, Y., Taburet, G., Dupuy, S., Pelloquin, C., Ablain, M., & Picot, N. (2016). DUACS DT2014: The new multi-mission altimeter data set reprocessed over 20 years. *Ocean Science*, *12*(5), 1067–1090. https://doi.org/10.5194/os-12-1067-2016

Quartly, G. D., Legeais, J. F., Ablain, M., Zawadzki, L., Joana Fernandes, M., Rudenko, S., et al. (2017). A new phase in the production of quality-controlled sea level data. *Earth System Science Data*, *9*(2), 557–572. https://doi.org/10.5194/essd-9-557-2017

Tebaldi, C., Strauss, B. H., & Zervas, C. E. (2012). Modelling sea level rise impacts on storm surges along US coasts. *Environmental Research Letters*, *7*(1). https://doi.org/10.1088/1748-9326/7/1/014032

Vignudelli, S., Kostianoy, A. G., Cipollini, P., & Benveniste, J. (Eds.). (2011). *Coastal altimetry*. Berlin, Heidelberg: Springer. https://doi.org/10.1007/978-3-642-12796-0

Vinogradov, S. V., & Ponte, R. M. (2011). Low-frequency variability in coastal sea level from tide gauges and altimetry. *Journal of Geophysical Research*, *116*, C07006. https://doi.org/10.1029/2011JC007034

Wahl, T., & Chambers, D. P. (2015). Evidence for multidecadal variability in US extreme sea level records. *Journal of Geophysical Research: Oceans*, *120*, 1527–1544. https://doi.org/10.1002/2014JC010443

Wöppelmann, G., & Marcos, M. (2016). Vertical land motion as a key to understanding sea level change and variability. *Reviews of Geophysics*, *54*, 64–92. https://doi.org/10.1002/2015RG000502

Zhang, K., Douglas, B. C., & Leatherman, S. P. (2000). Twentieth-century storm activity along the U.S. East Coast. *Journal of Climate*, *13*(10), 1748–1761. https://doi.org/10.1175/1520-0442(2000)013<1748:TCSAAT>2.0.CO;2